Reynolds Number and Impeller Diameter Effects on Instabilities in Stirred Vessels

C. Galletti and A. Paglianti
Laboratory of Process Equipment, Dept. of Chemical Engineering, Industrial Chemistry and Materials Science, University of Pisa, Via Diotisalvi 2, Pisa I-56126, Italy

K. C. Lee and M. Yianneskis
Experimental and Computational Laboratory for the Analysis of Turbulence, Division of Engineering, King's College London, Strand, London WC2R 2LS, U. K.

DOI 10.1002/aic.10236
Published online in Wiley InterScience (www.interscience.wiley.com).

*Flow instability phenomena in stirred vessels were studied with laser anemometry and flow visualization. The effects of fluid density and viscosity, impeller Reynolds number (*Re*), impeller design, diameter, and off-bottom clearance were investigated in order to quantify the frequencies (*f*) of the macroinstabilities stemming from precessional motions. The instabilities are characterized by two frequencies, one present at low* Re*, and another at high* Re *values. For intermediate* Re *values, both frequencies were present. In all cases,* f *was proportional to the impeller speed (*N*). The parameter* $f' = f/N$ *was shown to be linearly related to the impeller diameter in the low* Re *range;* f' *was not affected by impeller clearance. At constant* Re*, a change in fluid density and viscosity did not affect* f'. *The energy contained in the instability frequencies was shown to vary across the vessel. The implications of the results mixing practice are discussed.* © 2004 American Institute of Chemical Engineers *AIChE J,* 50: 2050–2063, 2004
Keywords: flow instabilities, precession, stirred vessel, fluid mixing, Reynolds number, impeller diameter.

Introduction

The flow patterns encountered in stirred vessels for different operational conditions and vessel/impeller geometries can critically affect the fluid mixing processes in such apparatus, and, consequently, process performance, and, therefore, accurate characterization of such patterns is essential for optimization of mixing process design (Tatterson, 1994). The flow fields are three-dimensional (3-D), more often than not turbulent, and their spatial and temporal features, such as the vortices trailing from the impeller blades (Yianneskis et al., 1987) and the instabilities of the flow structures (Hasal et al., 2000, Roussinova et al., 2000), introduce complexities that can affect mixing and circulation times and turbulence levels and, thus, make mixing process prediction and control a most complex task, and gross over-simplifications are often necessary. For example, the r.m.s. levels could be broadened, leading to erroneous estimation of the turbulence content (Yianneskis et al., 1987; Roussinova et al., 2000).

Although the trailing vortex structures and effects have been widely studied, knowledge of flow instabilities is far from complete. These instabilities can affect the mixing vessel performance in different ways, as pointed out by a number of studies. Haam et al. (1992) observed temporal variations in the local heat flux and heat-transfer coefficient at the wall of a stirred tank of up to 68%, which they attributed to the precession of an axial vortex structure moving relatively slowly in comparison to the impeller rotational speed. Further evidence

Correspondence concerning this article should be addressed to M. Yianneskis at michael.yianneskis@kcl.ac.uk

is provided by Houcine et al. (1999), who observed jet intermittence phenomena in the feedstream by means of a laser induced fluorescence (LIF) technique.

Different types of flow instability have been identified having different timescales. One instability stems from variation in the impeller off-bottom clearance. Even when the flow is stable, changes in the impeller stream inclination (Yianneskis et al., 1987), or in the flow pattern (Jaworski et al., 1991, Kresta and Wood, 1993) with variations in impeller clearance (C), have been reported for a Rushton turbine (RT) and a pitched-blade turbine (PBT), respectively. For some clearances, unstable flow patterns occur, however. Rutherford et al. (1996) studied a stirred tank equipped with two RTs, and found that the flow pattern depended on both the clearance and the separation between the impellers, identifying three stable and many unstable circulation patterns. In addition, flow variations stemming from the clearance of a single RT were identified by Montante et al. (1999), who established that the conventional double-loop circulation pattern occurred when $C/T > 0.20$, but the discharge flow became axial (single-loop) when the clearance was decreased to $C/T < 0.15$.

A second kind of instability is related to a change in impeller Reynolds number (Re). Nouri and Whitelaw (1990) found a transition due to Re variations in the flow pattern induced by a PBT for both Newtonian and non-Newtonian fluids. For Newtonian fluids, the flow pattern transition occurred at about $Re = 650$. This value was confirmed by the power number measurements carried out by Distelhoff et al. (1995). Hockey and Nouri (1996) measured the power number for a wide range of Re in a tank equipped with a PBT. A sudden drop in the power number was found when the Re was increased to 1,200, and it was shown by means of flow visualization that the direction of the discharge flow changed from radial to axial at this Re value. They explained the value of 1,200, which is around twice that previously established, by considering the difference in the PBT size: since the tank and impeller used by Hockey and Nouri (1996) were twice those used in the previous works (Nouri and Whitelaw, 1990, Distelhoff et al., 1995), the same V_{tip} corresponded to the two Re numbers. Schäfer et al. (1998) observed by means of flow visualization the flow discharged by a PBT to be directed axially at higher Re and radially at lower Re. The flowstream direction was unstable, varying from radial to axial, for Re around 500. Computational fluid dynamics (CFD) results have also shown a change in the flow pattern stemming from a variation in Re. For example, Bakker et al. (2000) predicted that, for the flow discharged by a PBT, the impeller stream direction was radial for low Re, but axial for $Re < 400$.

Finally, a third type of instability due to a precessional motion of a vortex around the shaft is often detected as a large time-scale variation in the mean flow (termed macroinstability - MI). Yianneskis et al. (1987) observed the aforementioned vortex for a RT moving around the shaft with a period of 10 s for an impeller rotational speed of $N = 300$ rpm ($f/N = 0.02$). In the following text, a nondimensional MI frequency $f' = f/N$ is used for convenience. Winardi and Nagase (1991) noticed large time-scale fluctuations in a stirred vessel equipped with a marine propeller. The work by Haam et al. (1992) cited earlier also referred to this kind of instability. Bruha et al. (1995) used a device called a "tornadometer" to estimate the macroinstabilities induced by a PBT, and they found a linear relation between their frequency f and the impeller rotational speed N, according to $f = c_1 + c_2 \bullet N$, where $c_1 = -0.009$ to -0.04 and $c_2 = 0.041-0.05$. In a later work (Bruha et al., 1996), they reported a linear dependence of the MI frequency on N ($f' = 0.043-0.048$) for Re values above 9,000. No macroinstabilities were noted for $Re < 200$, and an increase in f' was observed for $200 < Re < 9{,}000$. Montes et al. (1997) studied MIs induced by a PBT, and observed different values for f' depending on the impeller Reynolds number: $f' = 0.09$ for $Re = 1{,}140$ and $f' = 0.0575$ for $Re = 75{,}000$. Hasal et al. (2000) observed for a PBT an f' value of 0.087 for $Re = 750$ and $Re = 1{,}200$, and a value of 0.057 for $Re = 75{,}000$. In addition, they noticed that the fraction of the total kinetic energy carried by the MIs (relative magnitude) varied with the location inside the stirred vessel. Myers et al. (1997) used digital particle image velocimetry to investigate macroinstabilities in a stirred tank equipped with a PBT. They pointed out transients with a period ranging from 40 to 300 impeller revolutions ($f' = 0.003-0.025$). Guillard et al. (2000) carried out LIF experiments on a stirred tank equipped with two Rushton turbines, observing large time-scale oscillations of the concentration, induced by an interaction between the flows from the impeller and a baffle. Roussinova et al. (2000, 2001) performed experiments in two tank sizes, using various impeller types, clearances and working fluids. A value of $f' = 0.186$ was established for the $D/T = 0.5$ PBTs studied.

Recently, macroinstabilities were investigated by Nikiforaki et al. (2003), who used two different impellers (RT and PBT) having the same diameter $D/T = 0.33$. The frequency of macroinstabilities was found to be linearly related to the impeller speed with $f' = 0.015-0.020$. This value was independent of impeller clearance and design. In the aforementioned article, experiments were carried out using only one fluid, that is, water, and the impeller Reynolds number was $Re > 20{,}000$, thus, the flow might be expected to be fully turbulent. This f' value is in agreement with those reported in many of the aforementioned works, but the reasons for the wide range of f' values reported for different configurations are manifold: different measurement locations and impeller/vessel geometries have been considered in different studies, and there appears to be a substantial complexity of, and/or a number of possibly related flow phenomena.

The above brief review has shown that there are still many unresolved questions in relation to MI phenomena in stirred tanks and, as MIs can strongly affect mixing processes, improved knowledge of the related phenomena could be employed to improve mixing performance. The objective of this work was to shed light into such phenomena through extending the investigation on macroinstabilities to different working fluids, in order to establish the influence of physical properties, such as density and viscosity on the related phenomena, a wider range of impeller Reynolds numbers, and for different impeller types and sizes. In this manner, this work aims to quantify the effect of ρ, μ, Re and D on the MIs, in order to attempt to explain the different results reported in the literature, and provide a more thorough understanding and improved characterization of mixing processes involved.

Stirred Vessel Configuration and Measurement Techniques

Measurements were made in a cylindrical stirred vessel of diameter $T = 0.294$ m, equipped with four equally spaced

Table 1. Geometrical Details of the Impellers Studied

	RT	RT	PBT	RT
D [mm]	98	119.5	136	195
D/T [−]	0.33	0.41	0.46	0.66
H_b/T [−]	0.20	0.20		0.20
W_b/D [−]	0.25	0.25		0.25
W/D [−]			0.264	
t_b/D [−]	0.016	0.018	0.016	0.018

baffles of width $B = T/10$. The tank was placed inside a trough in order to minimize refraction effects, due to the vessel curvature. The liquid level was equal to the tank diameter ($H = T$). Since, as pointed out by Nikiforaki et al. (2003), the presence or absence of a lid has little effect on the macroinstabilities, a free surface configuration was used. The stirred tank was equipped with various impellers. Three RTs of different diameter (D/T = 0.33, 0.41 and 0.66), and a 4-blade 45° PBT of D/T = 0.46 were used. The geometrical details of the four impellers are listed in Table 1.

The D/T = 0.33 Rushton turbine was set at three different clearances (C/T = 0.15, 0.33, and 0.5). Two clearances were used for the D/T = 0.41 Rushton turbine (C/T= 0.15 and 0.5), and the PBT (C/T = 0.33 and 0.5). The largest Rushton turbine was studied only at C/T = 0.5. The impeller rotational speed was varied from 60–350 rpm.

Water and aqueous sucrose solutions with different sucrose content were used as working fluids to study the flows in a wide range of impeller Reynolds numbers. The viscosity of the fluids was measured with a rotational rheometer (ARES Rheometer by Rheometric Scientific). The ranges of Re investigated for each configuration are listed in Table 2.

Measurements were taken in different locations inside the tank, covering a region from r/T = 0.12 to 0.46, and from z/T= 0.25 to 0.95. Most of the measurements were taken in the vertical plane located midway two neighboring baffles (θ = 45°), but a few measurements were also taken for $0° \leq \theta \leq 90°$ for the PBT set at C/T = 0.33. All measurement location coordinates (r/T, z/T, and θ) are specified in the figure captions, and discussed in the relevant text where appropriate.

Measurements were taken with a single-component LDA system. A 514 nm wavelength beam was supplied by a 3W Argon Ion laser, and split by a diffraction grating unit, which also provided frequency shifting. A Dantec BSA was used to process the Doppler signals. A large number of samples (300,000–700,000) was recorded for each run. The data rate varied from 0.4–1.5 kHz. The errors in the mean velocity and r.m.s. values reported were estimated to be 1–2% and 5–10%, respectively, through extensive comparisons with earlier LDA data (for example, Lee and Yianneskis, 1998, and others), and an analysis of the individual error sources in the manner suggested by Durst et al. (1981). Velocity data were analyzed using a FFT technique performed through subroutines available in the Matlab software package. The randomness of particle arrival intervals made necessary the resampling of velocity-time data in order to obtain data evenly distributed in time, over which the FFT could be calculated. Data were interpolated and resampled using the same amount of samples taken during the LDA acquisition, thus, the resampling frequency corresponded to the mean data rate. Three different frequency resolutions (δf = 0.0075, 0.01, and 0.015 Hz) were tested in the spectral analysis to confirm that the resolution did not affect the frequencies reported.

Flow visualization experiments were also carried out using a light sheet obtained by a combination of lenses, including a cylindrical lens. For the visualization tests, the fluid was seeded with polystyrene particles of 800 μm mean diameter and the resulting images were recorded by a video camera.

Results

LDA Experiments

Impeller Reynolds Number Effects. First, radial velocity data were taken in the stirred tank equipped with the D/T = 0.33 Rushton turbine set at C/T = 0.5. The measurement volume was located close to the free surface (z/T = 0.90–0.95), at two different radial distances from the vessel axis (r/T = 0.12 and r/T = 0.17), and in a plane located midway between two neighboring baffles (θ = 45°). No significant differences between the results acquired in the two locations were observed which indicated the macroinstability phenomenon was present in both locations in the vessel. The variation of the intensity of the macroinstability across the entire vessel is discussed later in this section.

As already pointed out by Nikiforaki et al. (2003), the macroinstability frequency was found to be linearly related to the impeller rotational speed. However, an important and hitherto never reported difference in the proportionality constant arose when considering different impeller Reynolds numbers. In Figure 1 the variation of the nondimensional macroinstability frequency f' is reported against Re for different working fluids. The graph may be divided into three regions.

- Region 1 ($400 < Re < 6{,}300$), for which the frequency spectra exhibited a single peak linearly related to the impeller speed with a value of $f' = 0.106$.
- Region 2 ($6{,}300 < Re < 13{,}600$), for which the frequency spectra exhibited the presence of two different peaks, linearly related to the impeller speed with f' values of 0.106 and 0.015, respectively.
- Region 3 ($13{,}600 < Re < 54{,}400$), for which the frequency spectra exhibited a single peak with $f' = 0.015$, in agreement with the findings of Nikiforaki et al. (2003).

The three regions identified above may be considered to correspond to the laminar, transitional and turbulent regimes, respectively. However, such a classification must be made with extreme care, as it is well established that the extent of turbulent flow in a stirred vessel varies with not only Re, but also with the location in the vessel (Bittorf and Kresta, 2000): even if the flow near the impeller is turbulent, it may become transitional and even laminar with increasing distance from the

Table 2. Ranges of Impeller Reynolds Number Investigated for Each Configuration

Impeller	D/T [−]	C/T [−]	Re [−]
RT	0.33	0.15	500–9,800
		0.33	9,100–54,400
		0.5	500–54,400
	0.41	0.15	30–1,700
		0.5	130–53,500
	0.66	0.5	2,000–6,200
PBT	0.46	0.33	400–47,700
		0.5	400–34,700

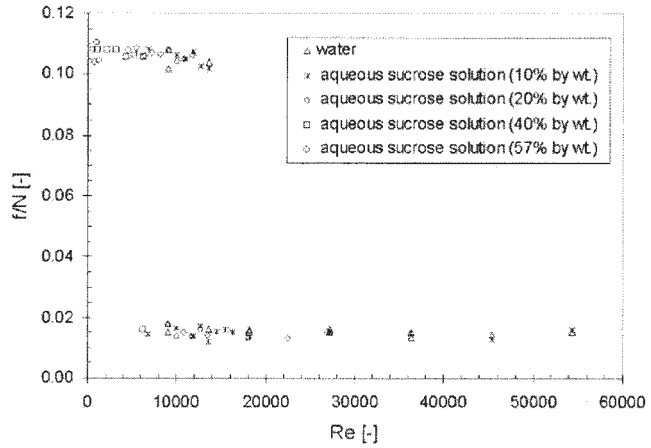

Figure 1. Nondimensional macroinstability frequency as a function of impeller Reynolds number for the *D/T* = 0.33 Rushton turbine set at *C/T* = 0.5, and using different working fluids.

Data obtained at $r/T = 0.12–0.29$, $z/T = 0.3–0.95$, $\theta = 45°$.

blades. Consequently, in order to avoid confusion, the characterization low, intermediate, and high *Re* regions is preferred, and used in the text later to denote the three regions identified earlier. The scatter in the data stems mainly from the frequency resolution employed, and is discussed further later.

Figure 2a illustrates a characteristic frequency spectrum obtained in region 3.

Measurements were taken with an aqueous sucrose solution with a sucrose content of 20 wt. %, using an impeller rotational speed of $N = 300$ rpm: the *Re* was 27,000. The peak frequency is $f = 0.075$ Hz ($f' = 0.015$), which corresponds to a period of 13.3 s. The cyclic variation of the macroinstabilities are illustrated in Figure 2b, where the instantaneous velocity is plotted vs. time, and the aforementioned 13.3 s period is clearly in evidence. The black continuous line was obtained by means of a moving-window-average technique, by calculating each average over 1,000 samples, and it shows visibly the cyclic variation.

Figure 3a shows the frequency spectrum obtained for the same working fluid, but using an impeller speed of $N = 60$ rpm in order to achieve the first (low *Re*) flow regime (*Re* = 5,400). The peak frequency is $f = 0.108$ Hz ($f' = 0.108$), thus, the period is 9.2 s. This period is indicated in the corresponding instantaneous velocity variation shown in Figure 3b. The moving-window-average technique to obtain the black continuous line was performed by calculating each average over 500 samples. In view of the low *Re* value for this case, it should be noted that the velocity fluctuations about the MI mean velocity variation appear large because the local velocities are small (of the order of 0.1 m/s), and the ordinate scale has been considerably expanded in relation to that of Figure 2.

A characteristic frequency spectrum acquired in the second (intermediate *Re*) regime ($N = 120$ rpm, *Re* = 10,800) is shown in Figure 4a. Two peaks of $f = 0.030$ Hz ($t = 33$ s) and $f = 0.210$ Hz ($t = 4.8$ s) can be clearly distinguished. The first peak corresponds to a nondimensional frequency value of $f' = 0.015$, identical to that noted earlier for the high *Re* region. The second peak corresponds to $f' = 0.105$, which is the same as that observed for the low *Re* region. The instantaneous velocity variation is illustrated in Figure 4b. The black continuous line was obtained by means of a moving-window-average technique, by calculating each average over 2,000 samples. In this manner, a cyclic fluctuation of a period of about 33 s can be identified. In addition, a more detailed observation points out the presence of a short period fluctuation superimposed to the one described earlier. Part of the time series of Figure 4b is enlarged in Figure 4c, where the instantaneous velocity is shown over a period of only 10 s: the black continuous line was obtained by means of the window-average technique over a lower number of samples (200). This enabled the detection of the short period cyclic fluctuation (4.8 s) related to the high frequency peak. The velocity data were analyzed in a similar

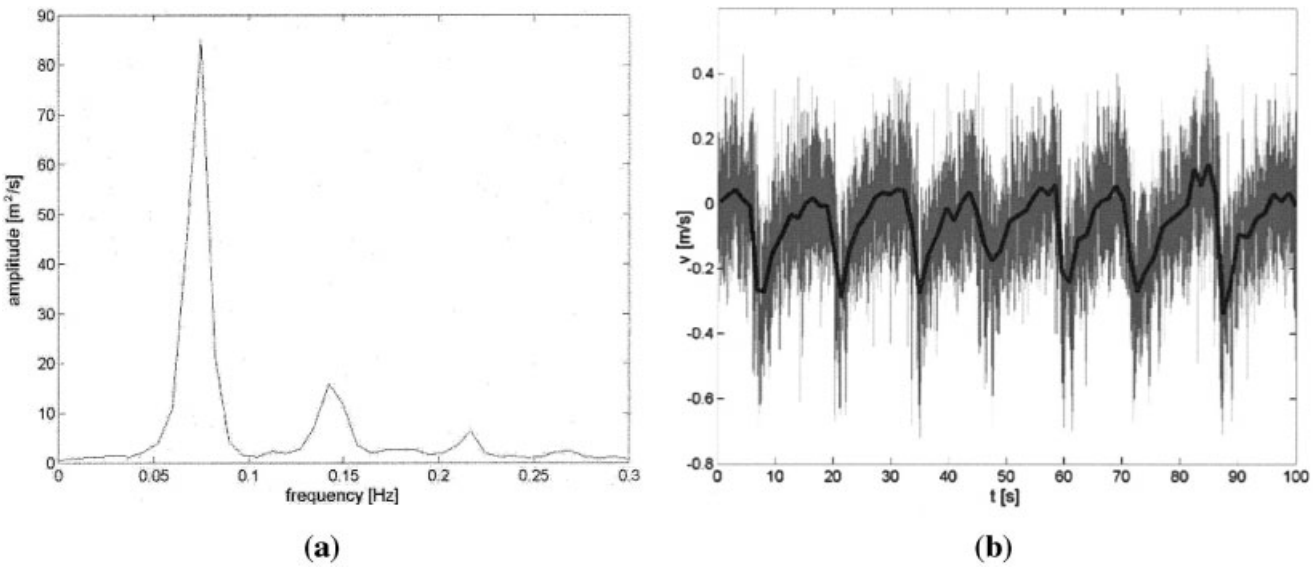

Figure 2. Rushton turbine, *D/T* = 0.33, *C/T* = 0.5, *N* = 300 rpm, *Re* = 27,000, *r/T* = 0.12, *z/T* = 0.90, $\theta = 45°$, $f' = 0.015$: (a) frequency spectrum, (b) time series.

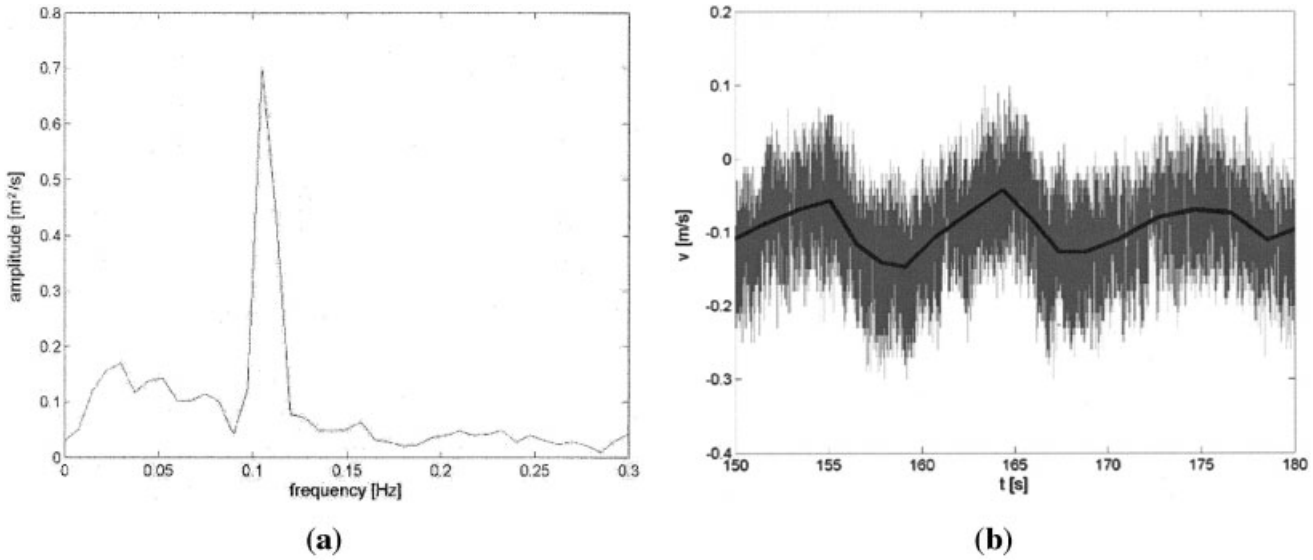

Figure 3. Rushton turbine, $D/T = 0.33$, $C/T = 0.5$, $N = 60$ rpm, $Re = 5{,}400$, $r/T = 0.12$, $z/T = 0.95$, $\theta = 45°$, $f' = 0.108$: (a) frequency spectrum, (b) time series.

manner over the entire range of impeller Reynolds numbers studied. The intermediate *Re* state was described as the one in which two peaks could be observed, and as previously mentioned, corresponded to $Re = 6{,}200–13{,}600$. Frequency spectra acquired in the intermediate *Re* region show that the relative amplitude of the two peaks varies with *Re*. The magnitude of the $f' = 0.108$ peak decreases with increasing *Re*, and this peak disappears for $Re = 13{,}600$. The two peaks have almost the same amplitude at $Re = 10{,}800$, as indicated in Figure 4a.

Effect of Fluid Properties. As stated previously, both water and different aqueous sucrose solutions were used, enabling an increase in the kinematic viscosity by about 40 times (from $8.8 \cdot 10^{-7}$ to $3.4 \cdot 10^{-5}$ m^2/s). As can be seen in Figure 1, the f' results obtained for different working fluids overlap when plotted in terms of *Re,* and this shows conclusively that the macroinstabilities are affected by *Re,* but not solely by a change in fluid properties, such as density and viscosity.

Effect of Impeller Off-Bottom Clearance. Measurements were also performed with the Rushton turbine placed at off-bottom clearances of $C/T = 0.15$, 0.33 and 0.5. The first configuration, as shown by Montante et al. (1999), leads to a single circulation loop, with the discharge flow directed axially. Figure 5 shows the macroinstability frequency values obtained against the impeller rotational speed for the 3 clearances. Some of the data can be fitted by a line with a steeper slope ($f' = 0.109$), and these are the data acquired in the first (low *Re*) region. The remaining data can be fitted by a line with a slope of $f' = 0.015$, and those were taken in the third (high *Re*) regime. It can be noted that data for the three different clearances both in the low and high *Re* regions overlap, indicating therefore, the clearance does not affect the macroinstability frequency. As far as the high *Re* region is concerned, this finding agrees with the work of Nikiforaki et al. (2003). Results for the $C/T = 0.33$ are found only in the $f' = 0.015$ group, since they were taken only in the third (high *Re*) region. The results obtained for different clearances for the $D/T = 0.41$ Rushton turbine, and the PBT are discussed later in this work, in the context of impeller diameter and design effects (Figures 6, 7, and 9), but they also show that neither *C* nor impeller design affect the f' values obtained.

Effect of Impeller-to-Tank Diameter Ratio. Velocity data were also taken with a larger Rushton turbine ($D/T = 0.41$) in order to establish the influence of the impeller size on the macroinstability frequency. The impeller was initially set at $C/T = 0.5$, and in Figure 6 the variation of f' with *Re* obtained for three of the different working fluids is presented. As already observed for the $D/T = 0.33$ Rushton turbine, the plot can be divided into three regions, corresponding to the low, intermediate and high *Re* regions. The intermediate *Re* region extends from $Re = 13{,}000$ to 20,000, so it is found at higher *Re* values with respect to the smaller ($D/T = 0.33$) Rushton turbine.

The nondimensional macroinstability frequency was $f' = 0.018$ for the high *Re* region. This value does not differ significantly from the one obtained with the smaller Rushton turbine. Moreover, the frequency resolution must be taken into account, since the finest resolution used in this work, that is, $\delta f = 0.0075$ Hz, is around 50% of the frequency of some of the high *Re* region peaks.

In contrast, the nondimensional macroinstability frequency obtained for the low *Re* region was $f' = 0.169$, thus higher than the result gained for the $D/T = 0.33$ Rushton turbine. This finding indicates an influence of the impeller-to-tank diameter ratio on the macroinstability frequency for the low *Re* region. It can be seen from Figure 6 that, as already mentioned in the previous section, a variation in fluid properties alone does not affect f', but it is *Re* that is the characteristic parameter.

Experiments were also performed with the $D/T = 0.41$ Rushton impeller placed at $C/T = 0.15$ (data not shown here for brevity, but contained in Figure 9) and they yielded identical f' values to those obtained with the higher clearance, both for the low and the high *Re* regions. This result confirms that impeller clearance does not affect the macroinstability frequency, as also noted for the smaller RT.

For a better understanding of the dependence of macroinstabilities on impeller size, measurements were also taken with a larger Rushton turbine ($D/T = 0.66$) in the low *Re* region. In

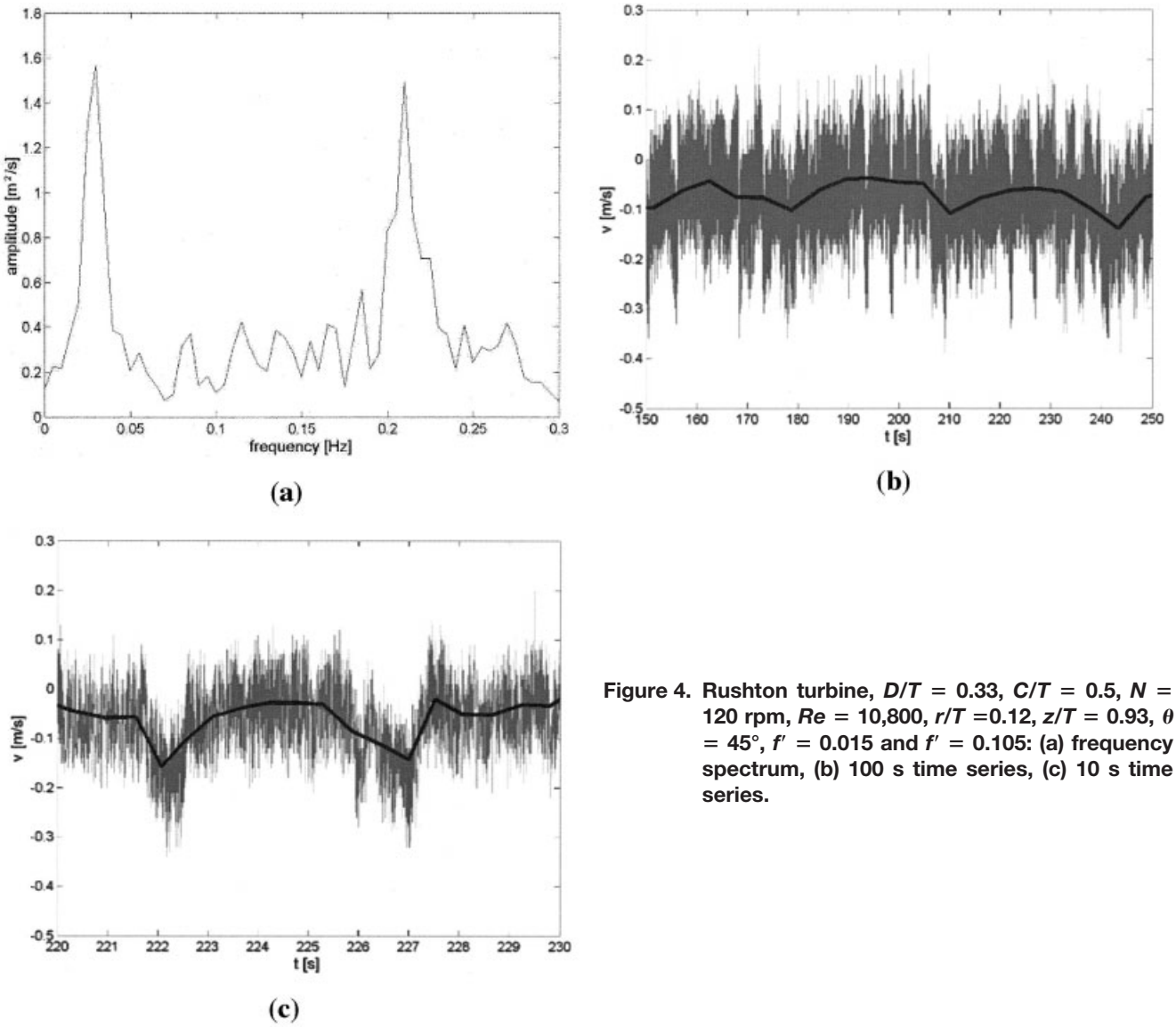

Figure 4. Rushton turbine, $D/T = 0.33$, $C/T = 0.5$, $N = 120$ rpm, $Re = 10{,}800$, $r/T = 0.12$, $z/T = 0.93$, $\theta = 45°$, $f' = 0.015$ and $f' = 0.105$: (a) frequency spectrum, (b) 100 s time series, (c) 10 s time series.

Figure 7, f results are plotted against the impeller rotational speed for the three Rushton turbines. For each impeller, data taken with different clearances are shown by means of open or filled symbols. Since, as shown in the previous section, the impeller off-bottom clearance does not affect the MI frequency, data taken with different C/T, but with the same D/T, have been interpolated by means of a single regression line, which is also illustrated in Figure 7. A set of data (shown by squares) acquired with the PBT in the low Re region is also shown: these data were obtained for two different off-bottom clearances ($C/T = 0.33$ and 0.5), but they can be fitted well by a single straight line. Thus, the clearance does not affect the frequency of the macroinstabilities induced by a PBT, as already observed for the RT. Moreover, it can be noted from Figure 7 that the slope of the lines increases with the impeller-to-tank diameter ratio. This is illustrated in Figure 8, where the nondimensional macroinstability frequency is plotted against D/T. The data can be fitted by a straight line given by an equation of the form

$$f' = a \cdot \left(\frac{D}{T}\right) + b \tag{1}$$

The constant values are $a = 0.83$ and $b = -0.17$. The correlation coefficient is 0.994. Therefore, as far as the low Re region and the RT data are concerned, the D/T ratio does affect the frequency of the macroinstability phenomena. The single D/T measurement with the PBT can also be described through Eq. 1, but the conclusion reached for the RT cannot be confirmed for this impeller without further measurements.

A similar analysis could not be carried out for the high Re region in a manner as accurate as for the low Re one, because the peak frequency values were lower, ranging from around 2–17 times the finest resolution used in the FFT analysis ($\delta f = 0.0075$ Hz). A linear dependence of the nondimensional macroinstability frequency on the impeller to tank diameter ratio was observed, and could be described by $f' = 0.068(\mathrm{D/T}) - 0.007$, however, the accuracy due to the frequency resolution

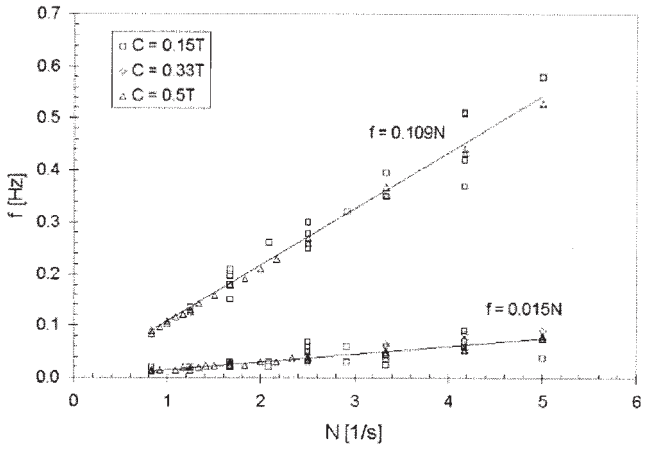

Figure 5. Macroinstability frequency as a function of impeller rotational speed for the *D/T* = 0.33 Rushton turbine set a three different clearances (*C/T* = 0.15, *C/T* = 0.33 and *C/T* = 0.5).

Data obtained at $r/T = 0.12–0.29$, $z/T = 0.3–0.95$, $\theta = 45°$.

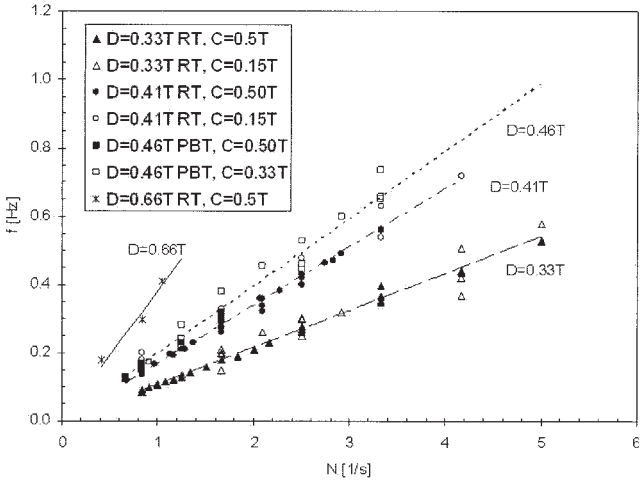

Figure 7. Macroinstability frequency as a function of impeller rotational speed for the different impellers in the low *Re* region.

Data obtained at $r/T = 0.12–0.46$, $z/T = 0.25–0.95$, $\theta = 45°$.

was not sufficient to draw firm conclusions on this variation. Moreover, results obtained for the two Rushton turbines ($D/T = 0.33$ and $D/T = 0.41$), and the PBT were all in the range $f' = 0.012–0.028$, thus, they cover a relatively small f interval.

It can be also observed from Figure 8 that macroinstability frequency results acquired for the $D/T = 0.46$ PBT fit well with those obtained with the three Rushton turbines for the low *Re* region. As regards to the high *Re* region, f' values obtained with the PBT are essentially identical to those obtained with the Rushton turbines. Therefore, both low and high *Re* region data show that impeller design does not affect the macroinstability frequency. This finding is in agreement with the work of Nikiforaki et al. (2003) who observed nondimensional macroinstability frequencies $f' = 0.011–0.022$ for both a Rushton turbine and a 6-bladed PBT with the same D/T ratio, and operating in the high *Re* region. This work confirms this finding and shows that it also applies to the low *Re* region.

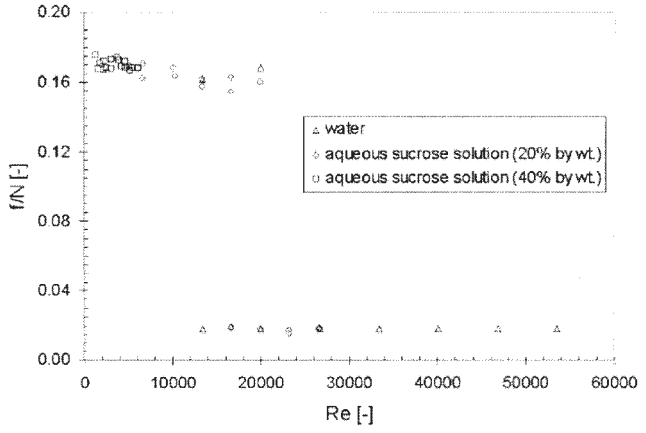

Figure 6. Nondimensional macroinstability frequency as a function of impeller Reynolds number for the *D/T* = 0.41 Rushton turbine set at *C/T*= 0.5 using different working fluids.

Data obtained at $r/T = 0.12–0.37$, $z/T = 0.3–0.95$, $\theta = 45°$.

In Figure 9, nondimensional macroinstability frequency data are plotted against impeller Reynolds number for all configurations investigated in this work, comprising different impeller types, sizes, and clearances. For some configurations, the experiments covered all three low, intermediate, and high *Re* regions. In this analysis, the existence of a dominant peak in the frequency spectrum was determined from the ratio of the power of the particular peak to those of other peaks in the low frequency region of the spectrum.

Two parameters that could be of interest for an improved understanding of the transition from the low to the high *Re* region macroinstability frequency are the range (ΔRe) over which the intermediate *Re* region takes place for the different cases studied, as well as the highest *Re* value for which the low *Re* region macroinstability peak is present ($Re_{max,low}$), and the lowest *Re* value for which the high *Re* region peak is found ($Re_{min,high}$). An exact quantification of such values would necessitate an even more extensive data set than the current one,

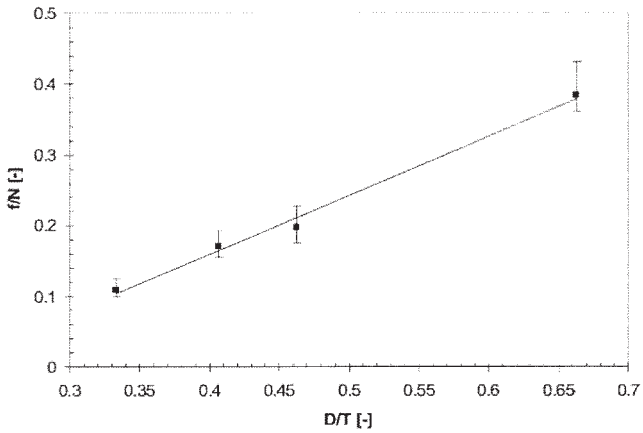

Figure 8. Nondimensional macroinstability frequency as a function of impeller to tank diameter ratio.

Rushton turbine and PBT. Data obtained at $r/T = 0.12–0.46$, $z/T = 0.25–0.95$, $\theta = 45°$.

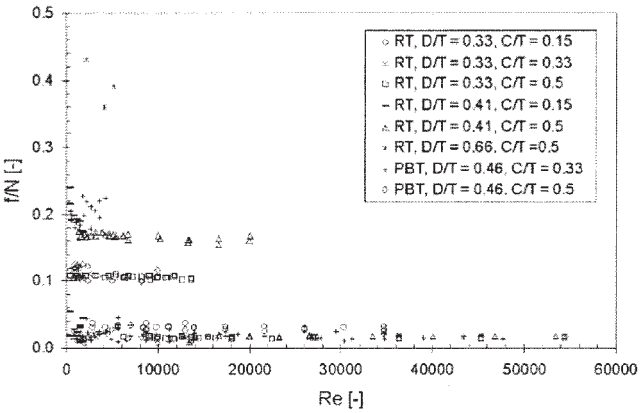

Figure 9. Nondimensional macroinstability frequency as a function of impeller Reynolds number for different configurations (impeller design, *D/T*, *C/T*).

Data obtained at r/T =0.12–0.46, z/T = 0.25–0.95, θ = 45°.

but indicative average values can be extracted from these data. For the D/T = 0.33 RT, $Re_{max,low}$ is on average around 13,000, and $Re_{min,high}$ 6,000, although with the D/T = 0.41 RT the corresponding values are around 20,000 and 13,000; in both cases, thus, the ΔRe range is approximately 7,000. With the PBT the intermediate *Re* region is encountered at much lower *Re* values, with $Re_{max,low}$ being on average around 2,000 and $Re_{min,high}$ 500, so that ΔRe is only around 1,500. It is emphasized, however, that the above values comprise only indicative averages for the cases studied.

Flow visualization experiments

Flow visualization was performed to acquire a better understanding of the macroinstability phenomenon, and especially to understand better the difference between macroinstability frequencies for the low and the high *Re* regions. The laser sheet was directed horizontally, and placed close to the free surface to visually observe the macroinstability phenomena near the surface of the liquid. Experiments were carried out for the D/T = 0.33, and the D/T = 0.41 Rushton turbines.

Long-term observations of the flow recordings showed that, at a fixed region near the shaft, the number of vortices crossing the region corresponded closely to the f' values reported earlier. This was the case for both the low and the high *Re* regions, and is illustrated in Figures 10 and 11.

Figure 10 shows images obtained in the stirred vessel with the D/T = 0.33 Rushton turbine set at C/T = 0.5, and using an aqueous sucrose solution with a sucrose content of 40 wt. %. The impeller was rotating clockwise with a rotational speed of 100 rpm. The impeller Reynolds number was 2,000; consequently, the low *Re* flow region was examined. The four video images shown were grabbed from the recorded tape at 1 s intervals, covering, thus, a total period of 3 s. In Figure 10 (1) two vortices can be observed. The vortex indicated by the green arrow is quite intense, whereas the second one, on the left side, and indicated by a red arrow, is weaker. The former vortex is developing and moving around the shaft, the distance of the vortex centre from the vessel axis being about 60 mm (r_v/T = 0.20) and its mean diameter around d_v = 30 mm

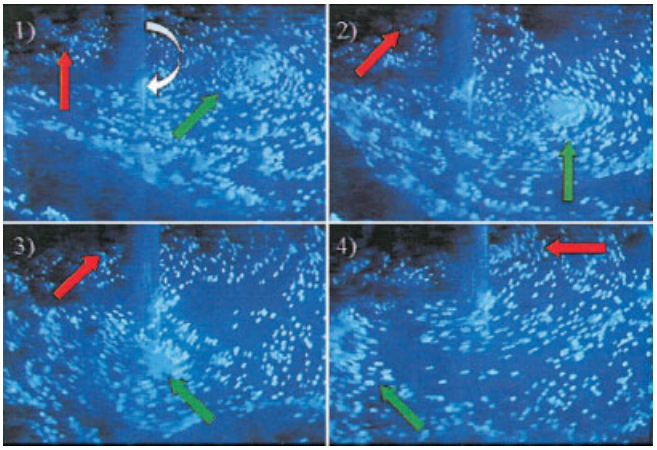

Figure 10. Flow visualization images taken every 1 s. Rushton turbine, *D/T* = 0.33, *C/T* = 0.5, *N* = 100 rpm, *Re* = 2,000.

(d_v/T = 0.10). The latter vortex is weaker and it is moving closer and toward the vessel axis, decaying as it approaches the shaft (Figure 10 (4)).

The frequency of the macroinstabilities could be approximately estimated by considering the path of the two vortices over a period of time, by

$$f = 2 \cdot \frac{v_v}{2 \cdot \pi \cdot r_v} = 2 \cdot \frac{(\theta_v \cdot r_v / t_v)}{2 \cdot \pi \cdot r_v} = \frac{1}{t_v} \cdot \left(\frac{\theta_v}{\pi}\right) \qquad (2)$$

In the above equation, v_v is the vortex velocity, and θ_v is the angle (in radians) covered by the vortices during the period t_v (3 s). The coefficient 2 takes into account the presence of two vortices moving around the shaft at the same time. For example, the circumferential angle travelled by a vortex in 3 s can be approximately estimated from Figure 10 as $\theta_v = 2\pi/3$. This value leads to a macroinstability frequency of f = 0.22 Hz, thus, f' = 0.13, which does not differ much from the expected value (f' = 0.108).

Figure 11 shows a similar flow visualization experiment for

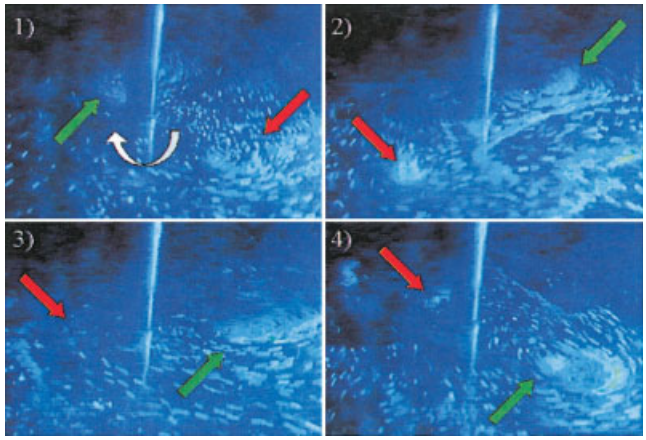

Figure 11. Flow visualization images taken every 1 s. Rushton turbine, *D/T* = 0.41, *C/T* = 0.5, *N* = 125 rpm, *Re* = 3,700.

the $D/T = 0.41$ Rushton turbine operating with the same fluid. The impeller speed was $N = 125$ rpm and, hence, the low *Re* region was observed ($Re = 3{,}700$). The images were again captured from the recorded video tape at 1 s intervals. As also observed for the smaller impeller, there are two vortices moving around the shaft at the same time. The mean diameter of the vortices is approximately 40 mm ($d_v/T = 0.14$), and the distance from the vessel axis of about 60 mm ($r_v/T = 0.20$). The first video image shows two vortices, one partly obscured by the shaft (indicated by the green arrow) and the other one on the right (red arrow). The vortices move around the shaft and complete almost half a revolution in 3 s. The vortex pointed by the red arrow decays in Figure 11(4). Applying Eq. 2, a frequency $f = 0.33$ Hz, and a nondimensional frequency $f' = 0.16$ is obtained (the value expected from the LDA data is $f' = 0.169$). The flow visualization showed that, when the impeller to tank diameter ratio is varied, no significant differences of the vortex locations and sizes could be observed. Nevertheless, it is difficult to provide an exact value of those parameters, since the vortices change position while moving around the shaft.

As far as the high *Re* region is concerned, the flow visualization was performed in the vessel filled with an aqueous sucrose solution with a sucrose content of 20 wt % and stirred by the smaller Rushton turbine ($D/T = 0.33$) placed at $C/T = 0.5$. The impeller speed was 200 rpm, leading to an impeller Reynolds number $Re = 17{,}600$ that corresponds to the high *Re* region for this configuration. The recording showed the presence of only a big vortex, which forms a whirlpool-type flow into the liquid. The laser sheet crosses the vortex and produces a large bright area, resulting in a lower quality images than for the earlier cases: such poor quality prevents from illustrating the images taken in the high *Re* region in this article. The vortex has a mean diameter of about 80 mm ($d_v/T = 0.27$), thus, it is much larger than the vortices observed for the low *Re* region. Its distance from the vessel axis is 70 mm ($r_v/T = 0.24$), consequently, it does not differ significantly from that for the low *Re* region. Moreover, this vortex lasts many seconds and it moves relatively slowly. From the images, it was derived that the vortex moves slowly and covers a circumferential angle of about $\pi/2$ in 6 s. For a similar analysis as provided earlier, Eq. 2 must be written in the form of Eq. 3 for the high *Re* region, because only a single vortex should be taken into account.

$$f = \frac{1}{2 \cdot t_v} \cdot \left(\frac{\theta_v}{\pi}\right) \tag{3}$$

When inserting $t_v = 6$ s and $\theta_v = \pi/2$ in the above equation, the resulting macroinstability frequency is $f = 0.042$ Hz and $f' = 0.013$.

The previous calculations have been made in an approximate manner, however, they facilitate a quantitative explanation of the difference between the macroinstability frequencies observed for the low and the high *Re* regions. For example, the $D/T = 0.33$ Rushton turbine exhibits a macroinstability frequency for the low *Re* region which is $0.108/0.015 = 7$ times higher than that obtained for the high *Re* one. Possible reasons for this difference between the two *Re* ranges is that the vortices move faster, or they travel a shorter path (that is, at smaller radii) in the same time, or that there is more than one vortex present. However, the flow visualization showed that the difference between the vortex center locations between the two flow regimes was not significant, and it clearly was not large enough to explain the difference, that is, the ratio of 7, in the macroinstability frequencies. The main observation that can be made from the flow visualization is that the low *Re* region is characterized by more than one vortex moving around the shaft at the same time. These vortices are quite small and they last a few seconds before decaying near the shaft. In contrast, in the high *Re* region there is a single big vortex, which has a longer lifetime and moves more slowly around the shaft. Even if the slightly larger radius at which the high *Re* case vortex is located is taken into consideration, this would only account for a frequency around 1.35 times lower than the low *Re* case. If a combined effect of the number of vortices and vortex center location (a factor of approximately 2.4) is considered, $7/2.4 = 2.9$, and this factor of 2.9 cannot be accounted for without further analysis and/or experimentation, but its probable origins are considered further in the Discussion section.

Variation of the intensity of macroinstabilities with location in the vessel

As established by previous works carried out by different researchers and with different techniques (LDA, PIV), macroinstabilities are not a local phenomenon and exert an influence over a large part of the stirred tank.

In this work, an area near the top of the vessel, that is, at the $z/T = 0.93$ level, was selected to carry out further velocity measurements with the $D/T = 0.33$ Rushton turbine set at $C/T = 0.5$, for both the high and the low *Re* regions. Velocity data were taken at different radial distances from the vessel axis, at spatial intervals of 10 mm.

The recorded data were studied by means of frequency analysis and the resulting spectra showed clear macroinstability peaks for radial positions close to the shaft, up to about 0.25T and 0.29T, for the low and the high *Re* regions, respectively. When moving the LDA measurement volume further nearer the walls, the frequency spectra became more spread, and they did not exhibit clear peaks. In Figure 12, the instantaneous velocity is plotted against time for different radial positions for the high *Re* region ($Re = 17{,}600$). The black continuous line was obtained by means of the moving-window-average technique, by performing each average over 1,000 samples. Figures 12a and 12b ($r/T = 0.12$ and 0.19, respectively) show a pronounced fluctuation. When moving toward the walls, the oscillations are less pronounced. However, the power spectrum of the data of Figure 12c ($r/T = 0.25$) also exhibited a clear peak. Finally, the recording of Figure 12d ($r/T = 0.36$) is uniform, and its spectrum did not show any macroinstability peak. This is in good agreement with the flow visualization observations, which revealed the presence of vortices moving around the shaft at distances from the vessel axis of about $r_v/T = 0.20$ and $r_v/T = 0.23$, for the low and the high *Re* regions, respectively.

As far as experiments carried out with the impeller placed at the lowest clearance ($C/T = 0.15$) are concerned, the frequency spectra of the velocity data recorded near the free surface did not allow the identification of a clear peak. This may be explained by considering that the impeller was located too far from the surface to produce sufficiently strong macroinstabilities in the top part of the vessel. In addition, the free surface appeared smooth and no vortices could be observed. However,

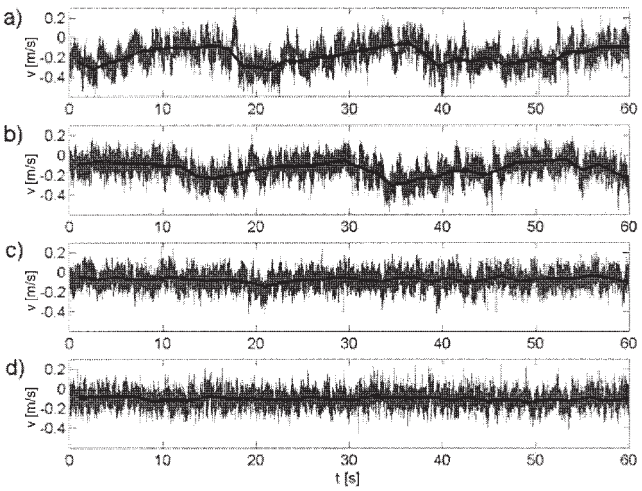

Figure 12. Time series acquired at $z/T = 0.93$, $\theta = 45°$.

Rushton turbine, $D/T = 0.33$, $C/T = 0.5$, $N = 200$ rpm, $Re = 17{,}600$: (a) $r/T = 0.12$, (b) $r/T = 0.19$, (c) $r/T = 0.25$, (d) $r/T = 0.36$.

as the measurement volume was moved closer to the impeller, that is, at the level $z/T = 0.30$, frequency spectra characterized by well-defined peaks were obtained.

As far as the PBT is concerned, since clearances of $C/T = 0.33$ and $C/T = 0.5$ were studied, peaks were identified in the frequency spectra of the data recorded near the free surface. However, the spectra were more spread compared to the ones obtained with the Rushton turbines, as previously noted by Nikiforaki et al. (2003), who observed many harmonics in addition to the main peak. In that work, this was considered to be due to the breaking up and reformation of the precessing vortex at irregular time intervals.

In this work, measurements were made in a vertical plane containing the vessel axis with the vessel stirred by a PBT set at $C/T = 0.5$. The working fluid was an aqueous sucrose solution with sucrose content of 57 wt. %. Velocity measurements were performed using impeller rotational speeds of 50, 100, and 200 rpm, corresponding to impeller Reynolds numbers of 500, 1,000 and 2,000, respectively. These values correspond to the low, intermediate, and high *Re* regions for the PBT, as indicated by the results shown earlier in Figure 9. Clearly, the value of $Re = 2{,}000$ is much lower than that of 20,000, which is normally considered as that above which turbulent flow is present in the vessel. Therefore, it should not be expected that the flow across the entire vessel is turbulent at $Re = 2{,}000$, and for this reason the PBT results were checked and repeated very carefully. The same peaks were found, which may indicate that at least at some regions in the vessel the transition to turbulence occurs at relatively low *Re* with the PBT. This may be partly related to, or triggered by, the change in the flow pattern due to the *Re* number. As cited in the introduction, many studies (Nouri and Whitelaw, 1990; Hockey and Nouri, 1996; Bakker et al., 2000) observed the flow discharged by a PBT to become radial when the impeller Reynolds number was decreased. The values of *Re* at which the transition occurred varied between different works, however, they were in the range of $Re = 400$–$1{,}200$. Since these values are close to those of this work, it may be assumed that a transition in the flow pattern occurs, leading to the observations of different frequency peaks. It would be interesting in future work to provide evidence of the flow pattern transition, and determine if there is a mechanism through which it affects the macroinstabilities. For $Re = 500$, only the frequency peak characteristic of the low *Re* region ($f' = 0.189$) was noted. For $Re = 2{,}000$, only a low-frequency peak ($f' = 0.034$) typical of the high *Re* region was observed. For $Re = 1{,}000$, both peaks could be distinguished in the frequency spectrum. Velocity data were taken in a rectangular grid at vertical levels of $z/T = 0.25$–0.95, and radial distances of $r/T = 0.12$–0.43, in 28 locations. The frequency spectra were analyzed to estimate the ratio of the amplitude of the macroinstability peak, and the background frequency content, to give an indication of its distribution. This is useful in order to establish the regions where macroinstabilities manifest themselves strongly, and can be easily detected.

Figure 13a shows, by means of a contour plot, the peak (a_{LP}) to background (a_B) amplitude ratio for the low *Re* region. The macroinstability peaks are more pronounced in the impeller region. Below the impeller, the peaks are less pronounced, but they can still be distinguished. Finally, above the impeller, the peaks are clearly defined for radial locations up to about $r/T = 0.2$, but less so nearer the vessel walls.

Before considering the intermediate *Re* region results in Figure 13b, it is instructive to examine Figure 13c, where the peak amplitude (a_{HP}) to background (a_B) ratio is illustrated for the high *Re* region. It can be observed that the macroinstability frequency peaks are well defined near the free surface, especially close to the shaft, while they are smaller near the shaft and the impeller. However, the MI peak amplitude is significant in the vessel bulk, even near the walls.

The dissimilarity between the contour plots obtained in low and high *Re* regions indicates a different behavior of the macroinstabilities. In the low *Re* region, the phenomenon seems to be more pronounced near the impeller, and weaker toward the free surface, strongly affecting a small region above the impeller around $r/T = 0.2$. In the high *Re* region, the macroinstability amplitude is less dominant near the impeller, extending to the walls and strongly affecting the free surface flow. This finding agrees with the flow visualization, which established the presence of a big vortex moving around the shaft near the surface for the high *Re* region, whereas smaller vortices were observed locally for the low *Re* region.

Figure 13b shows data at an impeller rotational speed of $N = 100$ rpm, which corresponds to the intermediate *Re* state, where two peaks in the frequency spectra were observed. The colored contour plot represents the ratio between the amplitude of the low- frequency peak (a_{HP}, characteristic of the high *Re* region) and the background (a_B). The contour lines refer to the low *Re* region; they show the values of the ratio between the high-frequency peak (a_{LP}, characteristic of the low *Re* region) and the background (a_B). It can be noted that the high *Re* case peak is stronger close to the shaft and the free surface, while the low *Re* peak is more concentrated in the impeller region. In conclusion, the relative importance of the two peaks depends on the location inside the vessel. Near the surface, and in the large part of the vessel bulk, the macroinstability phenomena are similar to those observed for the high *Re* region, whereas above and close the impeller, the low *Re* peak is dominant.

As mentioned in the introduction, the macroinstabilities in

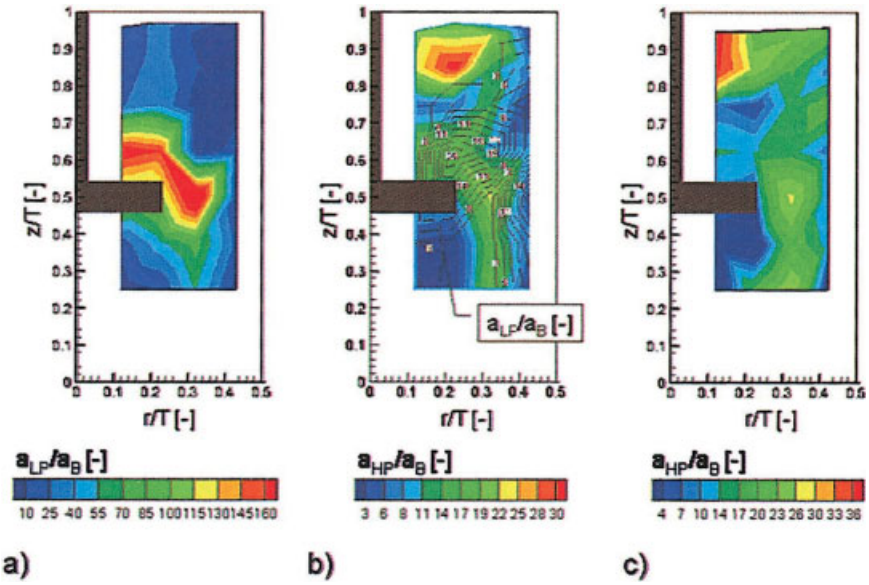

Figure 13. Contour plot of macroinstability peak magnitude to background ratio, for the PBT set at $C/T = 0.5$ using an aqueous sucrose solution (57 wt. %) as working fluid, for: (a) low *Re* region ($N = 50$ rpm, $Re = 500$); (b) intermediate *Re* region ($N = 100$ rpm, $Re = 1{,}000$); (c) high *Re* region ($N = 200$ rpm, $Re = 2{,}000$).

Data obtained at $r/T = 0.12–0.42$, $z/T = 0.25–0.95$, $\theta = 45°$.

stirred vessels equipped with a PBT have been widely investigated in literature (Bruha et al., 1995, 1996; Montes et al., 1997; Hasal et al., 2000; Myers et al., 1997; Roussinova et al., 2000, 2001; Nikiforaki et al., 2003), but the spread of the reported f' values is significant. As also pointed out in the introduction, this may be due to different flow phenomena, measurement locations, and/or approaches.

In this work, a further possible explanation of differences in f' was identified. To study this, the PBT was set at $C/T = 0.33$ in the vessel, which was filled with an aqueous sucrose solution of 40 wt. %. The impeller speed was $N = 200$ rpm, resulting in a $Re = 11{,}000$, which, according to the considerations made earlier for the PBT, should correspond to the high *Re* region. The impeller was rotating clockwise, as viewed from above a horizontal plane located at $z/T = 0.25$, was selected to carry out the velocity measurements, and, because of the internal symmetry of the vessel, just one-quarter of this plane (that is, an area described by an angle of 90°) was investigated. Velocity data were recorded in a measurement grid obtained by varying the location in steps of radial distance of 10 mm, and of polar angle of 15°. The shape of the frequency spectra associated to velocity data was analyzed for each location.

For many locations, the frequency spectra showed only the low frequency peak of $f' = 0.02$, characteristic of the high *Re* region, as the spectrum illustrated in Figure 14a. However, in a few locations a second peak with $f' = 0.18$ was observed. In Figure 14b a frequency spectrum with this latter peak is shown. In many locations, the frequency spectra exhibited both peaks. This is the case shown in Figure 15a. In addition, if a logarithmic-logarithmic representation is used as in Figure 15b and a single characteristic frequency is sought, the amplitude of the high frequency peak might be deemed as more clearly defined in relation to the lower frequency peak.

For a better understanding of the phenomenon, the amplitude ratio of the two peaks (a_{HF}, the high frequency over a_{HP}, the low frequency peak amplitude) was estimated for each location and illustrated through the contour plot shown in Figure 16. The region between two baffles could not be completely covered, because of lack of optical access. Values above 1, that is, colors from yellow to red, indicate that the $f' = 0.18$ peak is the dominant one. It can be noted that, although the low frequency peak is the dominant one over a large part of the investigated region, there is a significant region closer to the wall, where the high frequency peak amplitude is dominant. A possible reason is that the baffles cause the formation (shedding) of vortices behind them, leading to higher frequency phenomena. This could explain the high frequency peaks noted by many authors. For example, Roussinova et al. (2001) reported a peak of $f' = 0.18$ with a 45° PBT having $D/T = 0.5$, and they took measurements upstream of baffles for $z/T = 0.40–0.80$.

Discussion

The presence of macroinstabilities in stirred vessels may have beneficial implications for mixing process operation and efficiency, as such flow motions can enhance mixing through mean-flow variations. For example, the associated low-frequency, high-amplitude oscillatory motions in regions of low turbulence in a vessel, have the capability of transporting substances fed to a mixing process over relatively long distances (Larsson et al., 1996). In addition, MIs could have similar effects to those reported for laminar mixing in stirred tanks by Murakami et al. (1980), and Nomura et al. (1997): additional raising and lowering of a rotating impeller and/or the reversal of the rotation of an impeller produced unsteady mean flow motions that either destroyed segregated regions or preventing them from forming, and could produce desired mixing times with energy savings of up to 90% in comparison to normal impeller operation.

A thorough understanding of the parameters and mecha-

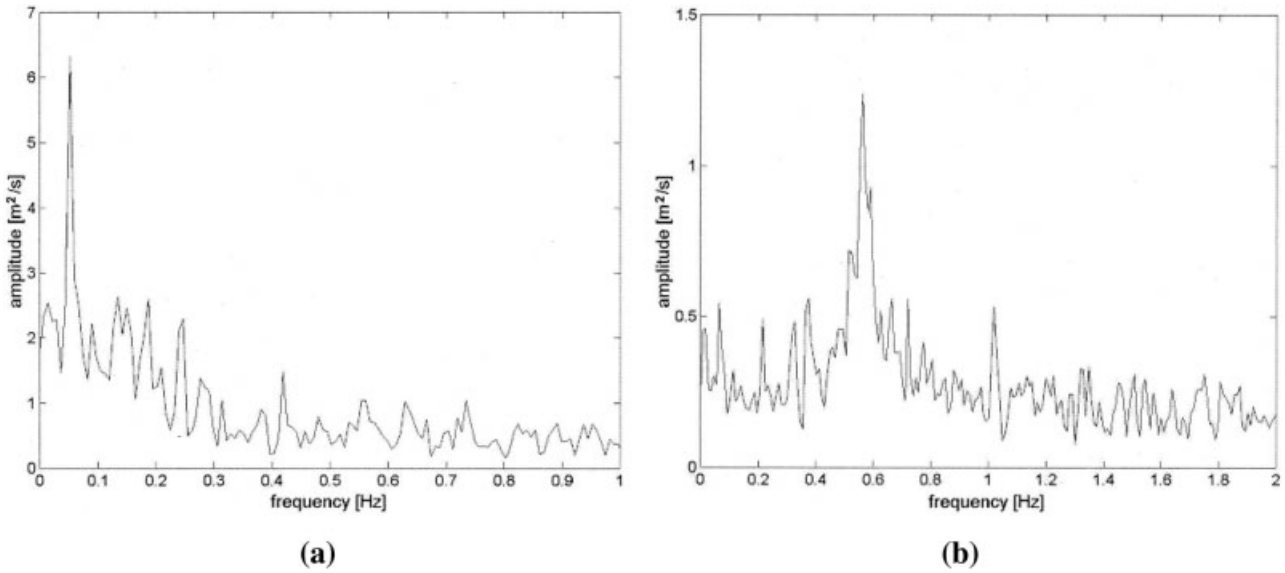

Figure 14. Frequency spectra of velocity data acquired with a PBT set at $C/T = 0.33$, using an aqueous sucrose solution (40 wt. %) as working fluid.

$N = 200$ rpm, $Re = 11{,}000$, $z/T = 0.25$: (a) $r/T = 0.31$, $\theta = 75°$, (b) $r/T = 0.41$, $\theta = 45°$.

nisms responsible for the generation and control of MIs could, therefore, aid the improvement of mixing process operation. The manifestation of the macroinstabilities has been indicated by this, as well as previous works (Yianneskis et al., 1987; Haam et al., 1992; Nikiforaki et al., 2003), as a precessional motion of one or more vortices around the shaft.

Vortex precession in swirling flows stems from a flow-induced precessional velocity, and the frequency of the precession is linearly related to the swirl intensity, while under certain flow conditions more than one precessing vortices may be present (Alekseenko et al., 1999). A stirred vessel comprises a swirling flow system of considerable complexity. A recent study on simpler systems, precessional radial jets induced by rotating bodies on thin layers (Vladimirov et al., 2001), reported the jet precessional speed to be linearly related to the propeller rotational speed. In that work a large variety of rotating bodies was investigated (propellers having different number of blades and disks), and it was established that the jet precessional speed is not affected by the rotating body design. This agrees with the findings of this work, where by means of experiments carried out with both a RT and a PBT, it was shown that impeller design does not affect the macroinstability

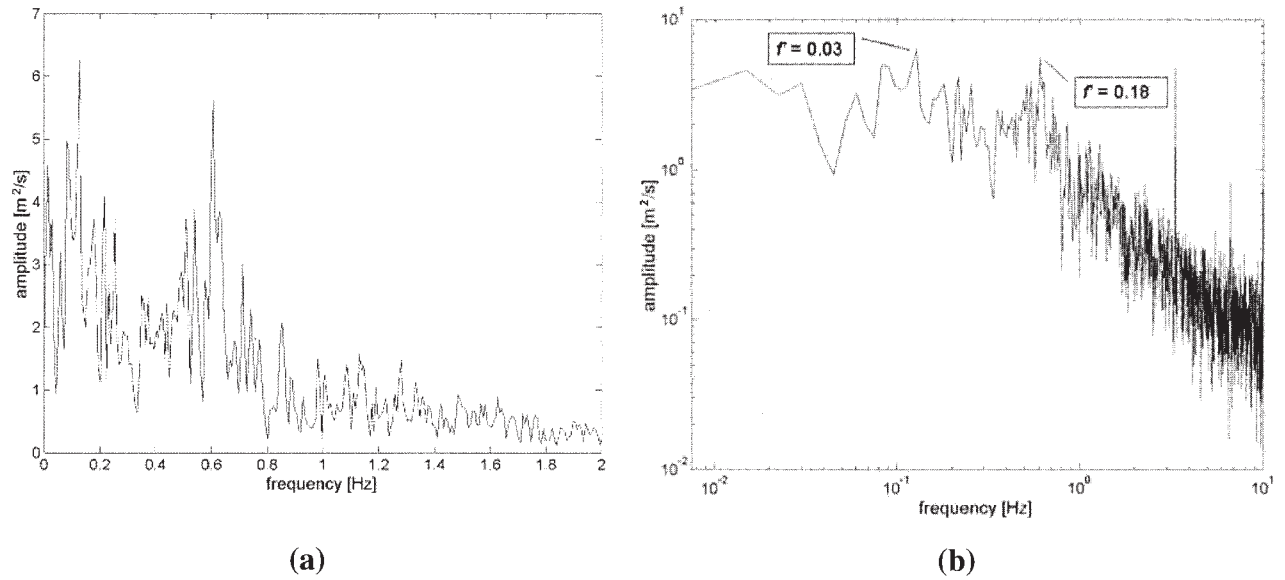

Figure 15. Frequency spectrum of velocity data acquired with a PBT set at $C/T = 0.33$, using an aqueous sucrose solution (40 wt %) as working fluid. $N = 200$ rpm, $Re = 11{,}000$, $z/T = 0.25$, $r/T = 0.26$, $\theta = 15°$: (a) linear plot, (b) logarithmic - logarithmic plot.

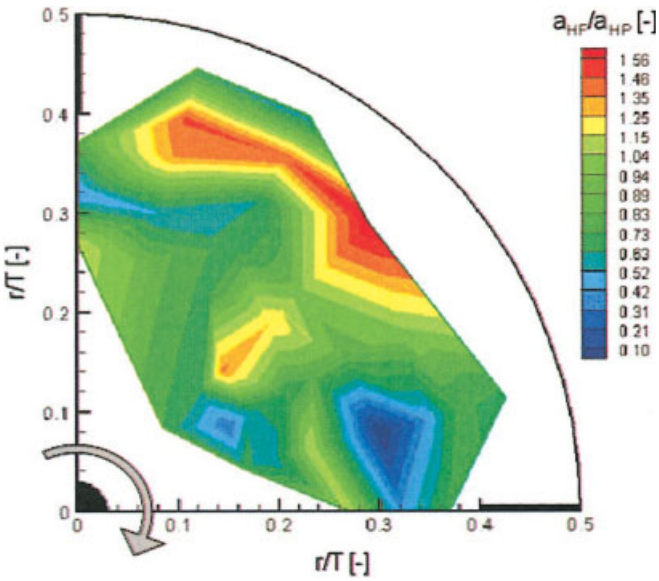

Figure 16. Contour plot of ratio of high frequency peak to high *Re* peak magnitudes for the PBT set at *C/T* = 0.33, using an aqueous sucrose solution (40 wt %) as working fluid.

Data obtained at $z/T = 0.25$, $r/T = 0.12$–0.46, $\theta = 0$–$90°$.

frequency. Moreover, Vladimirov et al. (2001) found that the proportionality constant between the jet precessional speed, and the rotating body rotational speed was dependent on the ratio between the rotating body diameter and the layer diameter, when the other geometrical parameters are constant. This dependence was only found for rotating body diameters larger than 0.1 times the thin layer diameter; this is the case of this work, as the above ratio may be replaced with the impeller to tank diameter ratio. These findings provide strong support for the conclusion that macroinstabilities in stirred vessels stem predominantly, if not exclusively, from the precessional motion of a vortex (or a number of vortices) around the shaft.

However, the reasons for the difference in the f' values found for low and high *Re* are not clear. Guo et al. (2001) studied turbulent swirling flow in a pipe downstream of a sudden expansion, and found that a precessing vortex was present for low swirl numbers (S) and an additional, around 10 times higher in frequency, oscillation, was superimposed to the lower-frequency precession for $S > 0.13$. The low-order precession almost stopped when $S = 0.17$, and reversed direction for $S > 0.22$, while the high-order one remained in the same direction. They suggested the latter might have been associated with vortex shedding. Although vortex shedding from baffle tips may affect the frequencies detected in this work, the effect of increasing N (and correspondingly S) is the opposite to that of Guo et al. (2001), and the low *Re* flows are essentially laminar.

There is no direct evidence that the MI phenomenon is coupled with the flow turbulence; an estimation of the integral turbulence time scale based on the direct measurements by Lee and Yianneskis (1998), indicates that the MI period is around 50 times higher and, therefore, the power contained in the MI peaks in the spectrum may be attributed to coherent fluctuations due to the precession. However, if in the high *Re* region the precessing vortex fluctuates more about its mean position in relation to low *Re* flow, this may provide some justification for the unaccounted for difference in the low and high *Re* region frequencies, and should be investigated further. The observed change in f' with *Re* range, and in particular the influence that the extent of low, intermediate, and high *Re* flows in stirred vessels has on this change, constitute important research questions that should be addressed in future work. Their significance for process prediction can be considerable because of the important effect turbulence can have on micromixing in particular.

Conclusions

In this work macroinstabilities have been studied using different working fluids, impeller types, diameters, and clearances. The already established linear dependence of the macroinstability frequency on the impeller rotational speed $f/N \approx 0.02$ was confirmed, however, it was found that macroinstabilities exhibited a different behavior when considering the low, intermediate, and high *Re* regions. This leads to different values of the proportionality constant. Specifically, it was found that in the low *Re* region macroinstabilities occurred with a nondimensional frequency about 7 times greater than that observed for the high *Re* region, for the case of the $D/T = 0.33$ Rushton turbine. For the high *Re* region, flow visualization established the presence of one big vortex that moves slowly around the shaft and lasts many seconds. For the low *Re* region, two small vortices moving relatively faster around the shaft and lasting just a few seconds before decaying near the shaft, were observed. When using different working fluids, no differences of the macroinstability frequencies were observed, indicating that the phenomenon is not affected by the fluid properties alone.

When different impeller off-bottom clearances were used, no significant variation in the macroinstability frequency was observed, therefore, the clearance should not exert any effect on the macroinstability, both for the low and the high *Re* regions. This finding was obtained both for the Rushton turbine and the PBT.

In contrast, a difference in the frequency was found when the impeller diameter was varied. This result was well established for the low *Re* region, and a linear dependence of the nondimensional macroinstability frequency on the impeller to tank diameter ratio was established $f' = a \cdot (D/T) + b$. A similar analysis could not be carried out as accurately for the high *Re* regime, because the peak frequencies were only a few times greater than the finest resolution used in the frequency analysis, preventing the formulation of a reliable relationship between f' and D/T. However, a similar relation to that above is indicated by the results, with a far smaller dependence of f' on D/T. In addition, it was established that impeller design does not affect the macroinstability frequencies both for the low and the high *Re* regions.

The data presented provide an improved characterization and understanding of macroinstability phenomena in stirred vessels. The mechanism of transition from the low to the high *Re* macroinstability frequency is not, however, fully understood and requires further study. In view of the potential benefits of MIs for the improvement of mixing efficiency in stirred vessels mentioned in the previous section, more exact knowledge of the mechanisms involved in their generation and control could supplement the optimization of mixing processes.

Notation

a, b = constants, Eq. 1
a_B = amplitude of the background in the frequency spectrum, m^2/s
a_{HF} = amplitude of the high frequency peak in the frequency spectrum, m^2/s
a_{LP} = amplitude of the low *Re* peak in the frequency spectrum, m^2/s
a_{HP} = amplitude of the high *Re* peak in the frequency spectrum, m^2/s
B = baffle width, m
C = impeller off-bottom clearance, m
c_1, c_2 = constants
D = impeller diameter, m
d_v = precessing vortex mean diameter, m
f = macroinstability frequency, Hz
f' = nondimensional macroinstability frequency, $f' = f/N$
H = liquid height, m
H_b = blade height for the Rushton turbine, m
N = impeller rotational speed, 1/s
r = radial co-ordinate measured from the vessel axis, m
Re = impeller Reynolds number, $Re = \rho \cdot N \cdot D/\mu$
$Re_{max,low}$ = highest impeller Reynolds number at which the low *Re* peak is present in the frequency spectrum of velocity data
$Re_{min,high}$ = lowest impeller Reynolds number at which the high *Re* peak is present in the frequency spectrum of velocity data
r_v = distance from the precessing vortex centre to the vessel axis, m
S = swirl number
T = tank inner diameter, m
t_b = disk and blade thickness, m
t_v = period of time in which the precessing vortex transcribes the angle θ_v, s
v_v = precessing vortex velocity, m/s
W = blade width for the PBT, m
W_b = blade width for the Rushton turbine, m
z = axial co-ordinate measured from the vessel bottom, m

Greek letters

δf = frequency resolution, Hz
ΔRe = range of impeller Reynolds numbers for which the low and high *Re* peaks are both present in the frequency spectrum of velocity data
θ = tangential co-ordinate of the angle measured from a baffle in clockwise direction, degrees
θ_v = angle covered by the precessing vortex during the interval of time t_v, radians
μ = dynamic viscosity, Pa · s
ρ = density, kg/m^3

Literature Cited

Alekseenko, S. V., P. A. Kuibin, V. L. Okulov, and S. I. Shtork, "Helical Vortices in Swirl Flow," *J. Fluid Mech*., **382**, 195 (1999).

Bakker, A., R. D. La Roche, M. Wang, and R. Calabrese, "Sliding Mesh Simulation of Laminar Flow in Stirred Reactors," *Published in The online CFM Book* at http://www.bakker.org.cfm (2000).

Bittorf, K., and S. Kresta, "Limits of Fully Turbulent Flow in a Stirred Tank," *Proc. 10th European Conf. on Mixing*, Delft, The Netherlands (2000).

Bruha, O., I. Fort, and P. Smolka, "Phenomenon of Turbulent Macro-Instabilities in Agitated Systems," *Collect. Czech. Chem. C.*, **60**, 85 (1995).

Bruha, O., I. Fort, P. Smolka, and M. Jahoda, "Experimental Study of Turbulent Macroinstabilities in an Agitated System with Axial High-Speed Impeller and with Radial Baffles," *Collect. Czech. Chem. C.,* **61**, 856 (1996).

Distelhoff, M. F. W., J. Laker, A. J. Marquis, and J. Nouri, "The Application of a Strain Gauge Technique to the Measurement of the Power Characteristics of 5 Impellers," *Exp. Fluids*., **20**, 56 (1995).

Durst, F., Melling, A., and J. H. Whitelaw, *Principles and Practice of Laser-Doppler Anemometry*, Academic Press, London (1981).

Guillard, F., Trägårdh, C., and L. Fuchs, "A Study of Turbulent Mixing in a Turbine-Agitated Tank using a Fluorescence Technique," *Exp. Fluids*, **28**, 225 (2000).

Guo, B., T. A. G. Langrish, and D. F. Fletcher, "Simulation of Turbulent Swirl Flow in an Axisymmetric Sudden Expansion," *AIAA J.,* **39**, 96 (2001).

Haam, S., R. S. Brodkey, and J. B. Fasano, "Local Heat-Transfer in a Mixing Vessel using Heat-Flux Sensors," *Ind. Eng. Chem. Res*., **31**,1384 (1992).

Hasal, P., J. L. Montes, H. C. Boisson, and I. Fort, "Macro-Instabilities of Velocity Field in Stirred Vessel: Detection and Analysis," *Chem. Eng. Sci.,* **55**, 391 (2000).

Hockey, R. M., and M. Nouri, "Turbulent Flow in a Baffled Vessel Stirred by a 60° Pitched Blade Impeller," *Chem. Eng. Sci.,* **51**, 4405 (1996).

Houcine, I., E. Plasari, R. David, and J. Villermaux, "Feedstream Jet Intermittency Phenomenon in a Continuous Stirred Tank Reactor," *Chem. Eng. J.,* **72**, 19 (1999).

Jaworski, Z., A. W. Nienow, E. Koutsakos, E., K. Dyster, and W. Bujalski, "An LDA Study of Turbulent Flow in a Baffled Vessel Agitated by a Pitched Blade Turbine," *Chem. Eng. Res. Des*., **69**, 313 (1991).

Kresta, S. M., and P. E. Wood, "The Mean Flow Field Producted by a 45° Pitched Blade Turbine: Changes in the Circulation Pattern due to Off Bottom Clearance," *Can. J. Chem. Eng*., **71**, 42 (1993).

Larsson, G., Tornkvist, M., Stahl Wernersson, E., Trägårdh, K., Noorman, H., and S.-O. Enfos, "Substrate Gradients in Bioreactors: Origin and Consequences," *Bioprocess. Eng.,* **14**, 281 (1996).

Lee, K. C., and M. Yianneskis, "Turbulence Properties of the Impeller Stream of a Rushton Turbine," *AIChE J*., **44**, 13 (1998).

Montante, G., K. C. Lee, A. Brucato, and M. Yianneskis, "Double- to Single- Loop Flow Pattern Transition in Stirred Vessels," *Can. J. Chem. Eng*., **77**, 649 (1999).

Montes, J. L., H. C. Boisson, I. Fort, and M. Jahoda, "Velocity Field Macro-Instabilities in an Axially Agitated Mixing Vessel," *Chem. Eng. J.,* **67**, 139 (1997).

Murakami, Y., T. Hirose, T. Yamato, H. Fujiwara, and M. Ohshima, "Improvement in Mixing of High Viscosity Liquid by Additional Up-and-Down Motion of a Rotating Impeller," *J. Chem. Eng. Jpn*., **13**, 318 (1980).

Myers, K. J., R. W. Ward, and A. Bakker, "A Digital Particle Image Velocimetry Investigation of Flow Field Instabilities of Axial-Flow Impellers," *J. Fluid. Eng*., **119**, 623 (1997).

Nikiforaki, L., G. Montante, K. C. Lee, and M. Yianneskis, "On the Origin, Frequency and Magnitude of Macroinstabilities of the Flows in Stirred Vessels," *Chem. Eng. Sci*. **58**, 2937 (2003).

Nomura, T., T. Uchida, and K. Takahashi, "Enhancement of Mixing by Unsteady Agitation of an Impeller in an Agitated Vessel," *J. Chem. Eng. Jpn*., **30**, 875 (1997).

Nouri, J. M., and J. H. Whitelaw, "Flow Characteristics of Stirred Reactors with Newtonian and Non-Newtonian Fluids," *AIChE J*., **36**, 627 (1990).

Roussinova, V. T., B. Grgic, and S. M. Kresta, "Study of Macro-Instabilities in Stirred Tanks using a Velocity Decomposition Technique," *Chem. Eng. Res. Des*., **78**, 1040 (2000).

Roussinova, V. T., R. Weetman, and S. M. Kresta, "Large Eddy Simulation of Macro-Instabilities in a Stirred Tank with Experimental Validation at Two Scales," *NAMF 2001*, (2001).

Rutherford, K., K. C. Lee, S. M. S. Mahmoudi, and M. Yianneskis, "Hydrodynamic Characteristics of Dual Rushton Impeller Stirred Vessels," *AIChE J*., **42**, 332 (1996).

Schäfer, M., M. Yianneskis, P. Wächter, and F. Durst, "Trailing Vortices Around a 45° Pitched-Blade Impeller," *AIChE J*., **44**, 1233 (1998).

Tatterson, G. B., Scaleup and Design of Industrial Mixing Processes, McGraw-Hill, New York (1994).

Vladimirov, V. A., V. I. Yudovich,M. Y. Zhukov, and P. V. Denissenko, "Asymmetric Flows Induced by a Rotating Body in a Thin Layer," *HIMSA Report*, University of Hull, UK (2001)

Winardi, S., and Y. Nagase, "Unstable Phenomenon of Flow in a Mixing Vessel with a Marine Propeller," *J. Chem. Eng. Jpn*., **24**, 243 (1991).

Yianneskis, M., Z. Popiolek, and J. H. Whitelaw, "An Experimental Study of the Steady and Unsteady Flow Characteristics of Stirred Reactors," *J. Fluid Mech*., **175**, 537 (1987).

Manuscript received Apr. 16, 2003, and revision received Dec. 18, 2003.